

Material properties of friction stir spot welded joints of dissimilar aluminum alloys

Chi-Sung JEON¹, Sung-Tae HONG², Yong-Jai KWON³, Hoon-Hwe CHO⁴, Heung Nam HAN⁴

1. Technical Research Center, Hyundai Steel Company, Dangjin 343-711, Korea;

2. School of Mechanical Engineering, University of Ulsan, Ulsan 680-749, Korea;

3. Department of Materials Science and Engineering, University of Ulsan, Ulsan 680-749, Korea;

4. Department of Materials Science and Engineering, Seoul National University, Seoul 151-744, Korea

Received 21 May 2012; accepted 9 October 2012

Abstract: Mechanical properties and material mixing patterns of friction stir spot welded (FSSW) joints of dissimilar aluminum alloys were investigated. Two aluminum alloys typically used in automotive applications, 5052-H32 and 6061-T6, were selected. During the experiment, the process parameters including the *z*-axis force and torque histories were measured as a function of the tool displacement. The mechanical properties were investigated by microhardness measurements of the joint, and the material mixing in the stir zone was investigated by EPMA. The experimental results illustrate different process parameter histories, material mixing in the stir zone and material properties including microhardness distributions for FSSW joints of dissimilar aluminum alloys, likely due to different mechanical behaviors of the selected aluminum alloys in the FSSW process temperature range.

Key words: friction stir spot welding; dissimilar aluminum alloys; force histories; torque histories; microhardness

1 Introduction

The recent effort to improve fuel efficiency in the automotive industry was reflected in the increased use of lightweight materials, especially aluminum and magnesium alloys. Among various aluminum alloys, 5xxx are commonly used for inner-body and trim panels in the automotive industry. Additionally, 6xxx aluminum alloys, which are generally cheaper than typical aerospace aluminum alloys and have better mechanical properties than 5xxx aluminum alloys, are receiving increasing in automotive industries.

Even though 6xxx aluminum alloys seem like a clear choice to fill the apparent gap between 5xxx aluminum alloys and more expensive aerospace aluminum alloys, 6xxx aluminum alloys are still costly. Therefore, manufacturing of all aluminum automotive parts using 6xxx aluminum alloys may not be feasible. Instead, using 6xxx aluminum alloys in the manufacture of only specific parts, which require improved mechanical properties, while still fabricating the

remaining parts using less expensive 5xxx aluminum alloys, could be a reasonable solution. However, it is well known that aluminum alloys show very poor weldability in the traditional fusion welding processes.

A typical traditional fusion welding process, resistance spot welding (RSW), which is the most commonly used joining technique for automotive parts made of steel sheets due to its low capital cost, ease of maintenance, and high tolerance to poor part fit up, has several technological challenges in joining aluminum alloys [1]. First, the electrode tip life is limited compared to welding steel sheets. Also, aluminum RSW is also likely to produce poor weld consistency [2,3]. The combined use of significantly dissimilar 5xxx and 6xxx aluminum alloys for automotive parts may exacerbate these problems.

The friction stir spot welding (FSSW) process, sometimes called spot friction welding (SFW) or friction spot joining (FSJ), is a derivative of the friction stir welding (FSW) process [4–6] invented by THOMAS et al [7] in 1991. Since FSSW and FSW are solid-state joining processes, melting is avoided during the process.

Therefore, both FSSW and FSW have the potential for joining various materials that are difficult or impossible to weld by conventional fusion processes. Also, for joining aluminum alloys, FSSW and FSW provide a weld zone, the strength of which is nearly identical to that of the base metal. In addition, since the energy input used for FSSW and FSW is relatively low, the size of the heat-affected zone (HAZ) and the residual stresses associated with the welds should be small [1]. An important difference between FSSW and FSW is that lateral movement of the tool is not involved during FSSW. As a result, the bonding mechanism for FSSW is quite different from that of FSW. Also, FSSW can be considered a transient process due to its short cycle time (usually a few seconds) [8,9].

Since the basic process of FSSW was first reported in 2001 [10], investigations of FSSW have been performed, including a comprehensive review [11] of the literature and FSSW of various dissimilar alloys. Until recently, most of the FSSW investigations of dissimilar alloys focused on the discussion of mechanical and microstructural properties of the joint. However, only a few studies included a discussion of the force and torque histories during the process, which are quite important in understanding the resultant material properties of the joint and eventually in the application of FSSW in practical manufacturing processes.

GERLICH et al [12,13] investigated the mechanism of tool penetration during FSSW of aluminum and magnesium alloy sheet materials, and explained the experimental results as a progression of wear events from mild wear (delamination) through severe wear and finally to melt wear of the material beneath the base of the rotating pin. Their experimental results also suggest

that the highest temperatures during FSSW of the selected aluminum and magnesium alloys are close to the solidus temperatures of each alloy.

In the present study, FSSW of two typical automotive aluminum alloys was investigated. Variation in force and torque histories during the whole FSSW process was first discussed in detail for four different combinations of aluminum alloys. The resultant heat input during the FSSW process for the four different combinations of aluminum alloys was also discussed. In addition, differences in material mixing in the stir zone of two dissimilar combinations of aluminum alloys were presented. The resultant microstructure and mechanical properties of the joint were briefly discussed.

2 Experimental procedures

In the present study, 3-mm-thick 5052-H32 and 6061-T6 aluminum alloy sheets were used. The chemical compositions and the mechanical properties at room temperature [14] of the selected aluminum alloys are listed in Tables 1 and 2, respectively. Lap joints of the selected aluminum sheets were fabricated by FSSW as schematically shown in Fig. 1(a), using the custom-made FSW/FSSW machine (TTI, USA) in Fig. 1(b). The FSSW process parameters and the geometry of the tool are listed in Table 3. In order to investigate the effect of the material combination on the properties of the FSSW lap joints, four different material combinations were selected, as listed in Table 4.

During the experiment, the spindle force (z -force) and torque along the z axis marked in Fig. 1(a) were measured as functions of the tool displacement. For a better understanding of variations in the z -force, torque,

Table 1 Chemical compositions of 5052-H32 and 6061-T6 aluminum alloys (provided by manufacturer)

Alloy	Composition (mass fraction)/%							
	Cr	Cu	Fe	Mg	Mn	Si	Ti	Zn
5052-H32	0.15–0.35	≤0.1	≤0.4	2.2–2.8	≤0.1	≤0.25		≤0.1
6061-T6	0.04–0.35	0.15–0.4	≤0.7	0.8–1.2	≤0.15	0.4–0.8	≤0.15	≤0.25

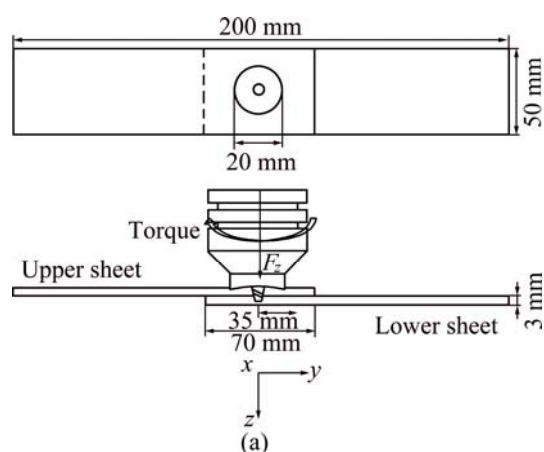
Table 2 Mechanical properties of 5052-H32 and 6061-T6 aluminum alloys [14]

Alloy	Ultimate tensile strength/MPa	Elongation/%	Yield strength/MPa
5052-H32	247	11.4	195
6061-T6	327	17.4	271

Table 3 Process parameters and tool geometry for FSSW of aluminum alloys

Rotation speed/ ($r \cdot \min^{-1}$)	Tool plunge depth/ mm	Control mode	Shoulder diameter/ mm	Pin diameter/ mm	Pin length ¹⁾ / mm	Shoulder type
750	4.55	Position control	20	6	4.2	concaved

1): At root of tapered pin.



(b)

Fig. 1 Schematic diagrams of experimental setup (a) and RM-1 FSW/FSSW machine (b)

Table 4 Material combinations for FSSW of selected aluminum alloys

Type No.	Notation	Top material (upper sheet)	Bottom material (lower sheet)
1	T5B5	Al 5052-H32	Al 5052-H32
2	T5B6	Al5052-H32	Al 6061-T6
3	T6B6	Al6061-T6	Al6061-T6
4	T6B5	Al6061-T6	Al5052-H32

and resultant heat input during FSSW of the selected material combinations, quasi-static tensile tests were conducted for the selected aluminum alloys at four different elevated temperatures, i.e. 200, 300, 400 and 450 °C, with a fixed displacement rate of 2 mm/min.

The weld microstructures were characterized based on experimental observations of the cross-section using optical microscopy, an electron probe micro analyzer (EPMA) and electron back scattered diffraction (EBSD). The cross-sections prepared from the FSSW joints of four different material combinations were ground, polished and etched by Keller's etch. The cross-sections of the FSSW joints were first examined using an optical microscope if the joints were successfully fabricated.

Additionally, as listed in Table 1, the 5052-H32 and 6061-T6 aluminum alloys have quite different Mg contents. Since no melting occurs during the FSSW process of aluminum alloys, the mixing of materials in the FSSW joints of the dissimilar aluminum alloys were investigated by mapping the Mg distribution in the joint [14]. In the present study, the distributions of Mg in the FSSW joints of the dissimilar combinations, T5B6 and T6B5 were analyzed using EPMA. Finally, EBSD was employed to examine the grain size distribution within the joint.

In order to evaluate the mechanical properties of the FSW joints, the hardness distribution within the joint was measured using a Vickers indenter under load of 981 mN for 10 s. The mechanical properties of the joints were also evaluated by quasi-static lap shear tests at room temperature with a displacement rate of 1 mm/min. The effects of material combinations on the failure load of the FSSW joints under quasi-static shear loads were briefly discussed.

3 Results and discussion

3.1 Force and torque histories and resultant heat input

The dissimilar 5052-H32 and 6061-T6 aluminum alloys were successfully joined with the selected FSSW parameters and no visible superficial porosity or macroscopic defects were observed for any of the four material combinations, as shown in Figs. 2(a), (b), (c), and (d). Figs 3(a) and (b) show representative Z-force and torque histories as a function of the tool displacement for the selected material combinations, which note that at least seven specimens were subject to FSSW for each material combination to ensure the repeatability of the force and torque histories. As shown in Figs. 3(c) and (d), the repeatability of the force and torque histories is quite good.

As shown in Figs. 3(a) and (b), the z-force and torque histories as functions of the tool displacement varied significantly during the FSSW process. In Figs. 3(a) and (b), three different stages (A, B and C) of the FSSW process are defined based on the contact phenomena between the tool and joined sheets during the process. Stage A indicates the period when the pin contacts the top surface of the upper sheet to when the pin contacts the top surface of the lower sheet. Therefore, during stage A, the pin of the rotating tool stays within the upper sheet, and contact between the tool shoulder and the upper sheet does not occur. As a result, the plastic flow, i.e. stirring of the material, primarily occurs within the upper sheet and the volume of the stirred material is relatively small.

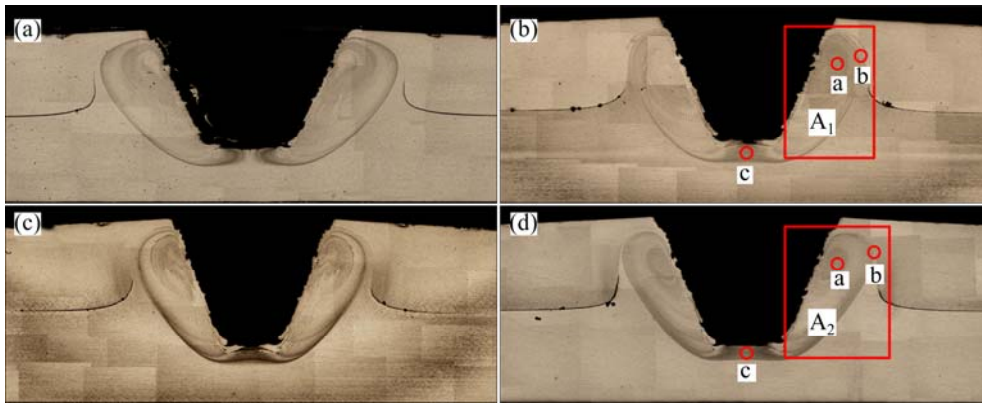


Fig. 2 Cross-sectional optical micrographs of T5B5 (a), T5B6 (b), T6B6 (c) and T6B5 (d) joints

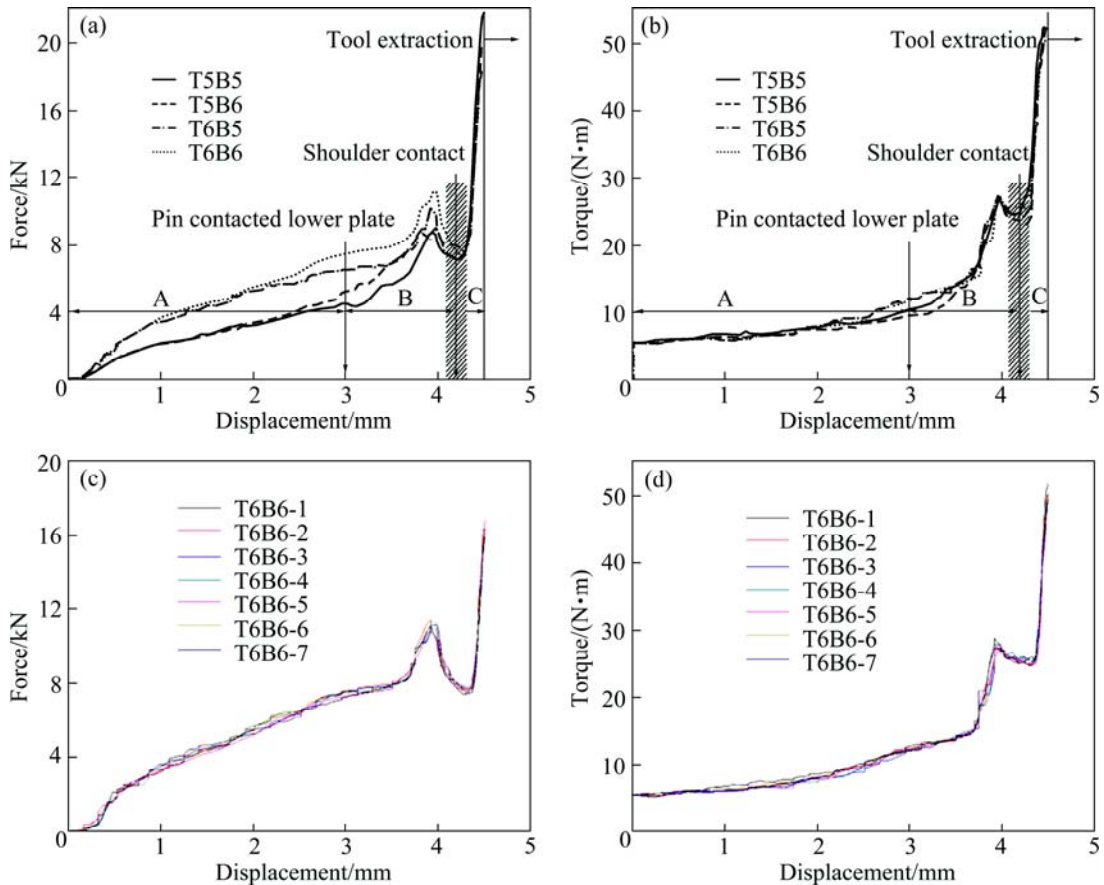


Fig. 3 Representative (a, b) and example (c, d) force (a, c) and torque (b, d) histories of FSSW joints

In stage B, the pin begins to plunge into the lower sheet. As a result, the materials in the upper and lower sheets begin to actively mix. Additionally, due to the tapered geometry and downward movement of the pin, the volume of the stirred material in stage B is greater than that in stage A. However, since the tool shoulder does not contact the upper sheet, the stir zone is still limited to near the tool pin.

In stage C, the shoulder of the tool makes contact with the upper sheet and as a result, the heat input and size of the stir zone increase significantly. Most of the

material mixing occurs during stage C. One thing should be noted is that the exact moment of contact between the tool shoulder and upper sheet is very difficult to find (marked as the shaded region in Figs. 3(a) and (b)) as the downward movement of the pin pushes the stirred material up around the pin [15].

The variations in the force and torque histories may be explained partially by quasi-static tensile behaviors of the two aluminum alloys at elevated temperatures, as shown in Figs. 4(a), (b), (c) and (d). However, the quasi-static mechanical behaviors at elevated temperature

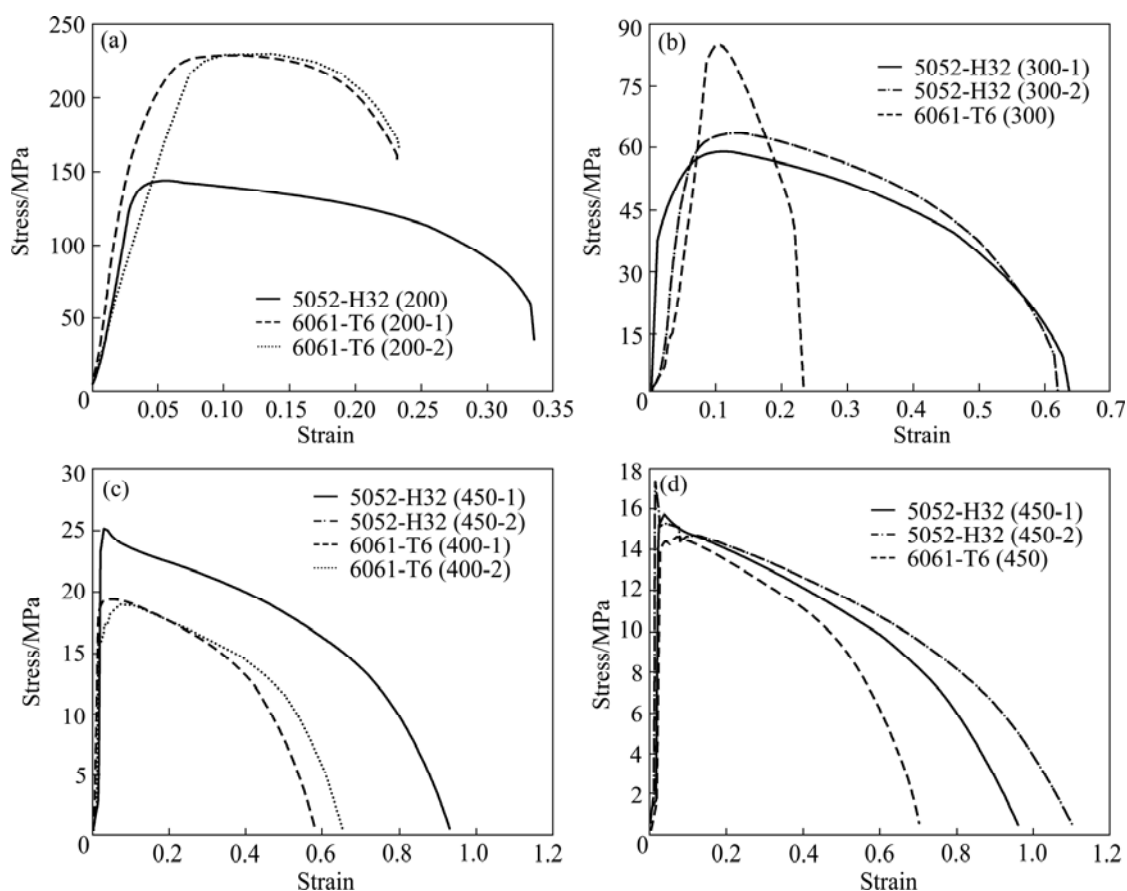


Fig. 4 Quasi-static tensile test results of aluminum alloys at elevated temperatures: (a) 200 °C; (b) 300 °C; (c) 400 °C; (d) 450 °C

may be used only as a broad guideline since the strain rate of the plastic flow during FSSW is extremely high.

For stage A, the variation in the force history strongly depends on the upper sheet material. The different variations in the force histories for the T5 combinations, T5B5 and T5B6, and T6 combinations, T6B5 and T6B6, are reasonable as expected by the different quasi-static mechanical behaviors observed when the two aluminum alloys were at elevated temperatures. It is interesting to note that the force histories with the same aluminum alloy in the upper sheet (for example T5B5 and T5B6) begin to deviate from each other as the pin gets closer to the lower sheet. The deviation of the force histories prior to the contact of the pin to the lower sheet suggests that the lower sheet material begins to be affected by the heat generated by the rotating pin even though the pin has not plunged into the lower sheet. Also, throughout the FSSW process, including stage A, the torque histories of the four different combinations show quite similar variations. According to FRIGAARD et al [16], the torque may be expressed as

$$M = \frac{2}{3} \mu \pi P R^3 \quad (1)$$

where M is the interfacial torque, μ is the friction coefficient, R is the surface radius, and P is the pressure distribution across the interface.

The similar variations of the torque histories for the four different FSSW combinations in spite of the different shapes of the Z -force histories may suggest that the frictional coefficients against the rotating tool are somewhat different for the two different aluminum alloys.

After the contact of the pin to the lower sheet (stage B), both the force and torque histories of all four material combinations increase rapidly as the tool moves further down, which indicates that the lower sheet material is still relatively colder (and consequently harder) than the upper sheet material, even though the lower sheet material is somewhat affected by the heat generated by the rotating pin in the upper sheet. The force and torque histories in stage B keep increasing until shoulder contact (stage C).

In stage C, the shoulder of the pin finally begins to contact the upper sheet and the contact area between the tool and material increases significantly. Naturally, as the tool keeps moving downward, both the force and torque histories increase drastically until the end of the process. The peak force during stage C tends to depend on the upper sheet material. Compare the peak forces of the T5

and T6 combinations. This is reasonable as during stage C, the reaction force and resultant frictional force should be generated primarily by the area and downward movement of the rotating tool shoulder.

The heat input during the FSSW process is one of the most critical process parameters as it significantly affects the resultant microstructure and mechanical properties of the joint [17,18]. According to PEW et al [19], SU et al [20] and LIN et al [17], the heat input can be calculated as follows.

Heat input by tool rotation (Q_{Ω}) is [19]:

$$Q_{\Omega} = \int_0^t M_z \left(\frac{2\pi v}{60} \right) dt \quad (2)$$

where M_z is the torque, N·m; v is the rotating speed, r/min; t is the FSSW process time, s.

Heat input by tool plunge (Q_f) is [20]

$$Q_f = \int_0^{t_p} F_z V_z dt \quad (3)$$

where F_z is the axial force, N; V_z is the plunge rate, m/s; t_p is the tool plunging time, s.

Total heat input (Q_t) is [17]

$$Q_t = Q_{\Omega} + Q_f = \frac{2\pi v}{60} \int_0^t M_z dt + V_z \int_0^{t_p} F_z dt \quad (4)$$

The heat input was calculated using Eqns. (2), (3), and (4). As listed in Table 5, for all the material combinations, the heat input by the rotation of the tool is significantly greater than that by the plunge of the tool. Therefore, for the given experimental results, the total heat input during the process can be approximated as

$$Q_t \approx Q_{\Omega} \quad (5)$$

Also, for the selected material combinations, the heat input for the material combination with the 5052-H32 aluminum alloy is always greater than that without the 5052-H32 aluminum alloy. This may confirm that the frictional coefficient of the 5052-H32 aluminum alloy is greater than that of the 6061-T6 aluminum alloy at the FSSW temperature and strain rate. As a result, the greater heat input of the T5B6 combination compared to the T6B5 combination is natural as most of the interface between the tool and material is located in the upper sheet.

Table 5 Heat input during FSSW of aluminum alloys

Joint	Rotation heat input/J	Tool plunge heat input/J	Total heat/J
T5B5	28963.3	29.3	28992.6
T5B6	25478.0	29.6	25507.6
T6B6	22233.2	35.4	22268.6
T6B5	24136.6	33.4	24170.0

3.2 Microstructure characterization

The EPMA results of the Mg distribution in the stir zones of the dissimilar material combinations, T5B6 and T6B5 (marked as A₁ and A₂ in Figs. 2(b) and (d)) are shown in Figs. 5(a) and (b), respectively. The Mg distributions in Figs. 5(a) and (b) suggest that FSSW of the two dissimilar combinations exhibits quite different material mixing in the stir zone. The EPMA results also show that, in the T6B5 combination, the lower sheet material (5052H-32, in light color) has been pulled into the center region of the stir zone, while the lower sheet material (6061-T6, in dark color) is only in the outer region of the stir zone in the T5B6 combination. The mechanism of these different mixing behaviors is not clearly understood yet. However, the different mixing of materials is likely due to the different flow stress and viscosity of the selected dissimilar aluminum alloys at the temperature and strain rate of the FSSW process.

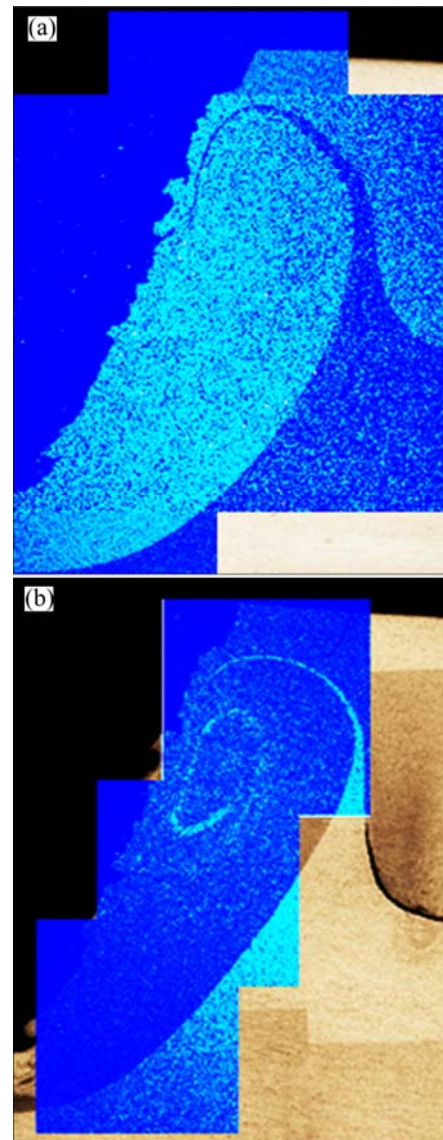


Fig. 5 Mg distributions in stir zone of T5B6 (a) and T6B5 (b) combinations

The EBSD analysis shows quite typical grain size distributions for FSSW joints of aluminum alloys [1,8, 21–24] as shown in Figs. 6 (a)–(c) and Figs. 7 (a)–(c). For the FSSW joints of the dissimilar combinations, extremely fine grains develop in the stir zone (Figs. 6(a) and 7(a)), while rather coarse grains developed in the thermomechanically affected zone (TMAZ, Figs. 6(b) and 7(b)). A discussion of the grain size in the stir zone TMAZ in comparison with the base metals (Figs. 8(a) and (b)) already has been provided by many other researchers [1,8,20–24] and will not be repeated here. Instead, the grain size of the regions under the pin (marked as c in Figs. 2(b) and (d)) is addressed here. As shown in Figs. 6(c), and 7(c), the grain size of the regions under the pin is the finest in the stir zone for both dissimilar FSSW joints. The finest grain size in the region c is likely due to the torsion zone underneath the pin [15]. In the torsion zone, the material is deformed in a manner of high-pressure torsion at an elevated

temperature.

3.3 Mechanical properties of joints

As shown in Figs. 9(a), (c) and (d), for the material combinations of T5B5, T6B6 and T6B5, Vickers hardness measurements reveal typical microhardness distributions, i.e., generally greater microhardness in the stir zone than in the TMAZ and HAZ for aluminum FSSW joints [18,21,23–25]. However, for the T5B6 combination (Fig. 8(b)), the microhardness of TMAZ and HAZ is still greater than that of the stir zone, likely due to the significantly greater strength of the 6061-T6 aluminum alloys than that of the 5052-H32 aluminum alloys as listed in Table 2.

Even though the T5B6 has a significantly different microhardness distribution compared to that of the other three material combinations, the failure mechanism of all the FSSW joints under quasi-static shear loads is strongly affected by the stress concentration induced by

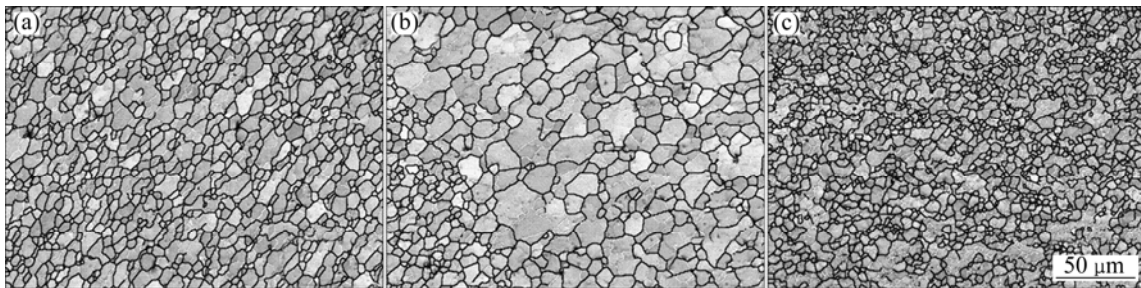


Fig. 6 Grain size distributions for T5B6 joint as marked in Fig. 2(b): (a) Stir zone, region a; (b) TMAZ, region b; (c) Torsion zone, region c

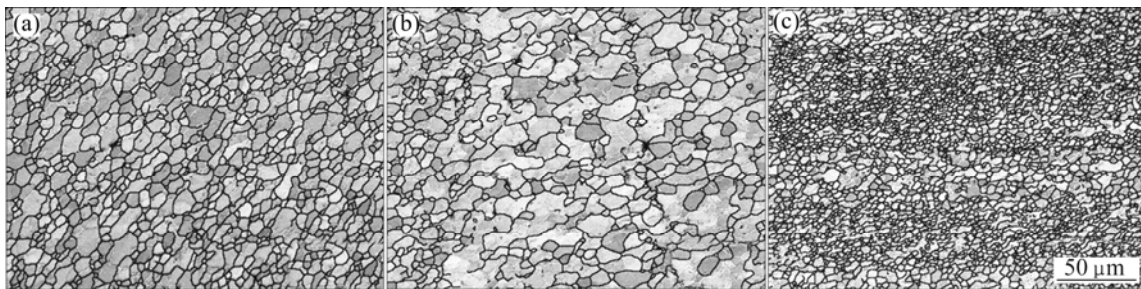


Fig. 7 Grain size distributions for T6B5 joint as marked in Fig. 2(d): (a) Stir zone, region a; (b) TMAZ, region b; (c) Torsion zone, region c

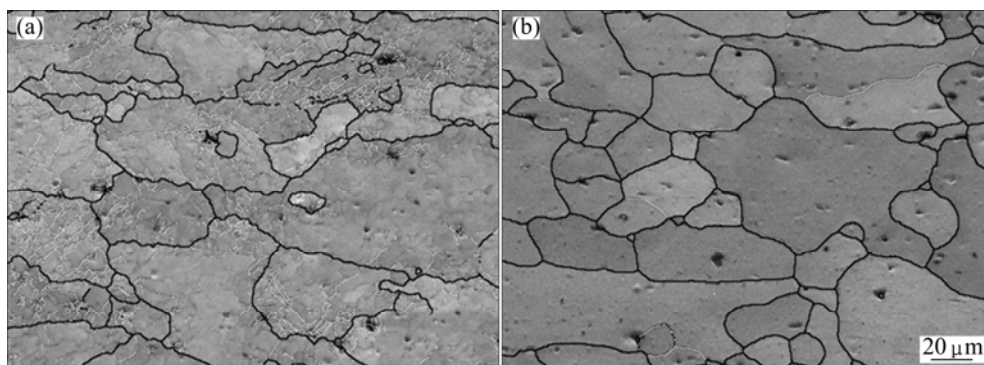


Fig. 8 Grain size distribution of base 5052-H32 (a) and 6061-T6 Al alloys (b)

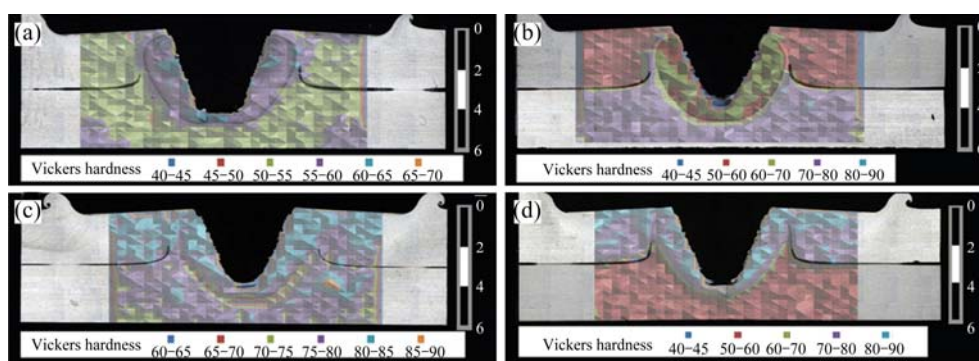


Fig. 9 Distribution of Vickers hardness of T5B5 (a), T5B6 (b), T6B6 (c) and T6B5 (d) joints

the hook near the stir zone [8,18,21,24,26]. As shown in Table 6, the T5B5 combination provides the highest shear load while the T6B6 combination provides the lowest shear load. Also, the displacement at the maximum shear load, which could be meaningful in practical applications, shows a similar trend. Both of the dissimilar combinations show similar maximum shear loads and displacements at the maximum shear load, which are close to the averages of the T5B5 and T6B6 combinations. It may be explained by that the failure of the lap FSSW joints under quasi-static shear loads is generally initiated at the hook, in which the interface is composed of materials from the upper sheet and lower sheet [9,27]. A detailed discussion regarding the failure mechanism of the FSSW joints of dissimilar aluminum alloys is beyond the scope of the present study and will be presented elsewhere.

Table 6 Results of quasi-static lap shear tests of FSSW joints

Joint	Maximum load/N	Displacement at maximum load/mm
T5B5	5732.9	1.82
T5B6	4855.8	1.24
T6B6	3618.7	0.92
T6B5	4710.0	1.30

4 Conclusions

1) The dissimilar 5052-H32 and 6061-T6 aluminum alloys were successfully joined with the selected FSSW parameters without visible superficial porosity or macroscopic defects. The z -force and torque histories as a function of tool displacement vary significantly during the FSSW process. The force and torque histories during the FSSW process can be distinguished by three different stages based on the contact phenomena between the tool and joined sheets. The shapes of the z -force histories are somewhat different for the selected material combinations, while the torque histories have quite

similar shapes. The differences in the z -force histories for the different material combinations may be explained based on the different mechanical behaviors of the aluminum alloys at various elevated temperatures.

2) The EPMA results of the Mg distribution in the stir zones of the dissimilar material combinations suggest that the FSSW of the two dissimilar combinations has quite different material mixing in the stir zone. The different mixing of materials is likely due to the different flow stress and viscosity of the selected dissimilar aluminum alloys at the temperature and strain rate of the FSSW process. The extremely fine grain size in the region underneath the pin may confirm a torsion zone during FSSW [15].

3) For the material combinations of T5B5, T6B6, and T6B5, Vickers hardness measurements reveal typical microhardness distributions for aluminum FSSW joints. However, for the T5B6 combination, the microhardness of TMAZ or HAZ is greater than that of the stir zone, likely due to the greater strength of the 6061-T6 aluminum alloy compared to the 5052-H32 aluminum alloy. In spite of the significantly different microhardness distributions of the T5B6 FSSW joint, the failure mechanism of all the FSSW joints under quasi-static shear loads is strongly affected by the typical stress concentration induced by the hook near the stir zone. The FSSW joints of the dissimilar combinations have similar maximum shear loads, and displacements at the maximum shear load as the failure of lap FSSW joints is generally initiated at the hook, the interface of which is composed of materials from the upper and lower sheets.

References

- [1] LIN P C, LIN S H, PAN J, PAN T, NICHOLSON J M, GARMAN M A. Microstructures and failure mechanisms of spot friction welds in lap shear specimens of aluminum 6111-T4 sheets [C]// 2004 SAE World Congress. Detroit City: 2004.
- [2] THORNTON P, KRAUSE A, DAVIES R. Aluminum spot weld [J]. *Welding Journal*, 1996, 175: 101–108.
- [3] GEAN A, WESTGATE S A, KUCZA J C, EHRSTORM J C. Static

- and fatigue behavior of spot-welded 51820 aluminum alloy sheet [J]. *Welding Journal*, 1999, 78: 80–86.
- [4] TOMOYUKI I. Method and apparatus for joining: US 6601751B2 [P]. 2003-08-05.
- [5] TOMOYUKI I. Method and apparatus for joining. EP 1 149 656 B1 [P]. 2005-10-19.
- [6] BADARINARAYAN H, HUNT F, OKAMOTO K. Friction stir spot welding, friction stir welding and processing [M]. MISHRA R S, MAHONEY M W. Ohio: ASM International, 2007: 235–272.
- [7] THOMAS W M, NICHOLAS E D, NEEDHAM J C, MURCH M G, TEMPLE SMITH P, DAWES C J. Friction stir butt welding. International Patent Application. PCT/GB92/02203 [P]. 1997-12.
- [8] BADARINARAYAN H, YANG Q, ZHU S. Effect of tool geometry on static strength of friction stir spot-welded aluminum alloy [J]. *International Journal of Machine Tools and Manufacture*, 2009, 49: 142–148.
- [9] BADARINARAYAN H, SHI Y, LI X, OKAMOTO K. Effect of tool geometry on hook formation and static strength of friction stir spot-welded aluminum 5754-O sheets [J]. *International Journal of Machine Tools and Manufacture*, 2009, 49: 814–823.
- [10] SAKANO R, MURAKAMI K, YAMASHITA K, HYOE T, FUJIMOTO M, INUZUKA M, NAGAO Y, KASHIKI H. Development of spot fsw robot system for automobile body members [C]// *Proceedings of 3rd International Symposium of Friction Stir Welding*. Kobe City: 2001.
- [11] PAN T Y. Friction stir spot welding (FSSW)—A literature review [C]// *2007 SAE World Congress*. Detroit City: 2007.
- [12] GERLICH A, YAMAMOTO M, SHIBAYANAGI T, NORTH T H. Selection of welding parameter during friction stir spot welding [C]// *2008 SAE World Congress*. Detroit City: 2008.
- [13] GERLICH A, SU P, NORTH T H. Tool penetration during friction stir spot welding of Al and Mg alloys [J]. *Journal of Materials Science*, 2005, 40: 6473–6481.
- [14] PARK S K, HONG S T, PARK J H, PARK K Y, KWON Y J, SON H J. Effect of material locations on properties of friction stir welding joints of dissimilar alloys [J]. *Science and Technology of Welding & Joining*, 2010, 15(4): 331–336.
- [15] YANG Q, MIRONOV S, SATO Y S, OKAMOTO K. Material flow during friction stir spot welding [J]. *Materials Science and Engineering A*, 2010, 527: 4389–4398.
- [16] FRIGAARD Ø, GRONG Ø, MIDLING O T. A process model for friction stir welding of age hardening aluminum alloys [J]. *Metallurgical and Materials Transactions A*, 2001, 32: 1189–1200.
- [17] LIN B Y, LIU J J, LU L D. Mechanical properties and fracture behavior of friction stir spot welded AZ61 magnesium alloys [J]. *Advanced Materials Research*, 2011, 154–155: 498–507.
- [18] YUAN W, MISHRA R S, WEBB S, CHEN Y L, CARLSON B, HERLING D R, GRANT G J. Effect of tool design and process parameters on properties of Al alloy 6016 friction stir spot welds [J]. *Journal of Materials Processing Technology*, 2011, 211: 972–977.
- [19] PEW J W, NELSON T W, SORENSEN C D. Torque based weld power model for friction stir welding [J]. *Science and Technology of Welding and Joining*, 2007, 12: 341–347.
- [20] SU P, GERLICH A, NORTH T H, BENDDZSAK G J. Energy generation and stir zone dimensions in friction stir spot welds [C]// *2006 SAE World Congress*. Detroit City: 2006.
- [21] BOZZI S, HELBERT ETTER A L, BAUDIN T, KLOSEK V, KERBIGUET J G, CRIQUI B. Influence of FSSW parameters on fracture mechanisms of 5182 aluminium welds [J]. *Journal of Materials Processing Technology*, 2010, 210: 1429–1435.
- [22] MITLIN D, RADMILOVIC V, PAN T, CHEN J, FENG Z, SANTELLA M L. Structure–properties relations in spot friction welded (also known as friction stir spot welded) 6111 aluminum [J]. *Materials Science and Engineering A*, 2006, 441: 79–96.
- [23] WANG D A, LEE S C. Microstructures and failure mechanisms of friction stir spot welds of aluminum 6061-T6 sheets [J]. *Journal of Materials Processing Technology*, 2007, 186: 291–297.
- [24] ZHAOHUA ZHANG, XINQI YANG, JIALONG ZHANG, GUANG ZHOU, XIAODONG XU, BINLIAN ZOU. Effect of welding parameters on microstructure and mechanical properties of friction stir spot welded 5052 aluminum alloy [J]. *Materials and Design*, 2011, 32: 4461–4470.
- [25] DA SILVA A A M, ALDANONDO E, OLARAN I, ALVAREZ P, ECHEVERRÍA A. Effect of joining parameters on performance of similar and dissimilar AA5754-H22 and AA6082-T6 friction stir spot welded aluminium alloys [C]// *SAE 2010 World Congress*. Detroit City: 2010.
- [26] PAN T Y, SANTELLA MICHAEL L, BLUNDELL N. Friction stir spot welding for structural aluminum sheets [C]// *2009 SAE World Congress*. Detroit City: 2009.
- [27] YIN Y H, IKUTA A, NORTH T H. Microstructural features and mechanical properties of AM60 and AZ31 friction stir spot welds [J]. *Materials and Design*, 2010, 31: 4764–4776.

(Edited by LI Yan-hong)